Eur Radiol (2006) 16: 2153–2160
DOI 10.1007/s00330-006-0276-4

Tadeusz W. Stadnik
Hendrik Everaert
Smitha Makkat
Robert Sacré
Jan Lamote
Claire Bourgain

Breast imaging. Preoperative breast cancer staging: comparison of USPIO-enhanced MR imaging and 18F-fluorodeoxyglucose (FDC) positron emission tomography (PET) imaging for axillary lymph node staging—initial findings

Received: 13 September 2005
Revised: 8 February 2006
Accepted: 31 March 2006
Published online: 3 May 2006

T. W. Stadnik (✉) · S. Makkat
Department of Radiology,
Academisch Ziekenhuis Vrije
Universiteit Brussel,
Laarbeeklaan 101,
1090 Brussels, Belgium
e-mail: stadnik@vub.ac.be
Tel.: +32-2-4775319
Fax: +32-2-4775362

H. Everaert
Department of Nuclear Medicine,
Academisch Ziekenhuis Vrije
Universiteit Brussel,
Brussels, Belgium

R. Sacré · J. Lamote
Department of Surgery,
Academisch Ziekenhuis Vrije
Universiteit Brussel,
Brussels, Belgium

C. Bourgain
Department of Anatomopathology,
Academisch Ziekenhuis Vrije
Universiteit Brussel,
Brussels, Belgium

Abstract Magnetic resonance (MR) imaging after ultra-small super paramagnetic iron oxide (USPIO) injection and 18F-fluorodeoxyglucose positron emission tomography (FDG-PET) for preoperative axillary lymph node staging in patients with breast cancer were evaluated using histopathologic findings as the reference standard. USPIO-enhanced MR and FDG-PET were performed in ten patients with breast cancer who were scheduled for surgery and axillary node resection. T2-weighted fast spin echo, T1-weighted three-dimensional (3D) gradient echo, T2*-weighted gradient echo and gadolinium-enhanced T1-weighted 3D gradient echo with spectral fat saturation were evaluated. MR imaging before USPIO infusion was not performed. The results were correlated with FDG-PET (acquired with dedicated PET camera, visual analysis) and histological findings. The histopathologic axillary staging was negative for nodal malignancy in five patients and positive in the remaining five patients. There was one false positive finding for USPIO-enhanced MR and one false negative finding for FDG-PET. A sensitivity (true positive rate) of 100%, specificity (true negative rate) of 80%, positive predictive value of 80%, and negative predictive value of 100% were achieved for USPIO-enhanced MR and of 80%, 100%, 100%, 80% for FDG-PET, respectively. The most useful sequences in the detection of invaded lymph nodes were in the decreasing order: gadolinium-enhanced T1-weighted 3D gradient echo with fat saturation, T2*-weighted 2D gradient echo, T1-weighted 3D gradient echo and T2-weighted 2D spin echo. In our study, USPIO-enhanced T1 gradient echo after gadolinium injection and fat saturation emerged as a very useful sequence in the staging of lymph nodes. The combination of USPIO-enhanced MR and FDG-PET achieved 100% sensitivity, specificity, PPV and NPV. If these results are confirmed, the combination of USPIO MR with FDG-PET has the potential to identify the patient candidates for axillary dissection versus sentinel node lymphadenectomy.

Keywords Breast neoplasms · Contrast media, comparative studies · Lymphatic system, neoplasms · Magnetic resonance (MR), contrast enhancement

Introduction

Treatment strategy and outcome in patients with breast cancer is dependent on axillary lymph node staging. Lymph node status is one of the most important prognostic factors in breast cancer [1]. To be of value for clinical decision making, the accuracy of any imaging modality used to assess axillary nodes must closely match that of histopathologic findings.

The current assessment of lymph node metastases by imaging is based mainly on measurement of nodal dimensions, such as maximum short axis diameter [2, 3] or ratios of maximum longitudinal to maximum short axis diameter [4]. The enhancement pattern and shape are further criteria with less importance.

Luciani et al. [5] found that the best discrimination between pathologic and negative findings were the presence of irregular contours, high signal intensity on T2 and marked gadolinium enhancement.

Brown et al. [6] found that if a node was defined as suspicious because of an irregular border or mixed signal intensity, a superior accuracy was obtained and resulted in a sensitivity of 85% and a specificity of 97%.

Superparamagnetic iron nanoparticles have been developed as contrast agents for magnetic resonance (MR) lymphography [7–9].

Studies of patients with head and neck, urologic, and pelvic cancers have confirmed the potential for improved detection of lymph node metastases by using USPIO-enhanced MR imaging when compared with nonenhanced or gadolinium-enhanced MR imaging [10–12].

The improved sensitivity and specificity (82 and 100%, respectively) of USPIO-enhanced MR was also reported in preoperative assessment of axillary lymph nodes in patients with breast cancer [13].

In another study, Stets et al. [14], using a lymph node diameter of >6 mm and visual assessment of signal change on T2-weighted spin echo, achieved 81% sensitivity and 92% specificity.

Additionally, 18F-fluorodeoxyglucose positron emission tomography (FDG-PET) imaging is also increasingly used in the staging of patients with metastatic disease.

Therefore, the aim of our prospective study was to evaluate USPIO-enhanced MR imaging and FDG-PET imaging for preoperative axillary lymph node staging in patients with breast cancer by using histopathologic findings as the standard of reference.

Materials and methods

Study design

This study was designed as a prospective, nonrandomized phase III off-license comparative trial of USPIO-enhanced MR imaging and FDG-PET imaging with a standardized protocol. Ten units of Sinerem (Guerbet, Roissy, France) were available for this trial. Women scheduled for mastectomy with axillary lymph node resection were considered to be enrolled in the study.

This selection bias with respect to the usual sentinel node procedure in breast cancer treatment was accepted in order to allow an optimal correlation between MR imaging, PET and pathology.

Exclusion criteria were a generally accepted contraindication for MR imaging, strong allergic disposition to gadolinium and/or to dextrans or drugs containing iron salts, as well as impossibility to obtain PET (for technical or accessibility reasons). The institutional review board approved the study, and written informed consent was obtained from all patients. The USPIO injection was performed only after final confirmation by the surgeon to perform axillary lymph node resection. The post-USPIO MR could be performed in all recruited patients and by October 2004 all ten studies could be completed.

MR imaging

The iron oxide nanoparticles coated in low molecular weight dextran (Sinerem, Guerbet, Roissy, France) were administered intravenously 24–36 h prior to MR imaging as a slow drip infusion (2.6 mg of iron per kilogram of body weight, diluted in 100 ml of 0.9% saline solution). The flow rate was adjusted approximately to 3 ml/min.

All MR examinations were performed with a 1.5-T magnet (Intera; release 8; Philips Medical Systems, Best, The Netherlands).

A double loop surface array coil was positioned on the axillary area with the patient in the supine position. The following sequences were performed in the transverse plane:

- T2-weighted 2D spin-echo images (repetition time ms/echo time ms, >3,500/90; echo train length, 18; section thickness, 3 mm; field of view, 260 mm; matrix, 256×256; voxel side, 1×1 mm; number of acquisitons, three; imaging duration, 5 min).
- T1-weighted 3D gradient echo (repetition time ms/echo time ms, >670/4,6; echo train length, 1; section thickness, 3 mm; field of view, 260 mm; matrix, 256×256 voxel side, 1×1 mm; number of acquisitons, three; imaging duration, 6 min).
- T2*-weighted 2D gradient echo (repetition time ms/echo time ms/flip angle, 120/15/25; echo train length, 1; section thickness, 3 mm; field of view, 260 mm; matrix, 256×256; voxel side, 1×1 mm; number of acquisitons, two; imaging duration, 6 min).

After i.v. injection of gadolinium [0.1 mmol of gadopentetate dimeglumine (Magnevist; Schering, Berlin, Germany) per kilogram of body weight], a T1-weighted 3D gradient echo with spectral fat saturation (repetition time

ms/echo time ms, >1,200/4,6; echo train length, 1; section thickness, 3 mm; field of view, 260 mm; matrix, 256×256; voxel side, 1×1 mm; number of acquisitons, two; imaging duration, 8 min) was also performed.

We tried to minimize the breathing artefacts by applying an oblique saturation pulse on underlying lung and heart.

We did not attempt to perform combined axillary lymph nodes and breast MR imaging (including dynamic pre- and postgadolinium acquisition).

PET imaging

Patient preparation and tracer administration

Patients were fasted for at least 6 h. Prior to tracer administration, an intravenous line was inserted and the blood sugar level was checked. Activities ranging from 370 to 536 MBq/kg ^{18}F-FDG, were administered (average 464±56 MBq). Ten minutes after tracer administration, 40 mg furosemide was given and patients were hydrated with 1 l of 0.9% saline solution over 50 min.

Imaging acquisition and reconstruction

Imaging was performed with patients in the supine position and arms placed above the head.

Whole body images corrected for attenuation were acquired with a LSO PET camera (Ecat Accel, Siemens) 60 min after tracer administration according an interleaved protocol. Emission data were obtained in 3D mode over 3 min per bed position. For transmission, ^{68}Ge sources (3×74 MBq; decay corrected) were used and data were acquired in 2D mode over 2 min per bed position.

Emission data were reconstructed iteratively (OSEM two iterations, 16 subsets), corrected for scatter and a post-reconstruction filter (6 mm Gauss) was applied. Filtered backprojection was used for the transmission, the constructed attenuation map was subsequently segmented into regions with similar attenuation factors. This segmented image was then forward projected to obtain attenuation correction factors for each line of response.

Image analysis

The MR images were analyzed in consensus by two radiologists (T.S. and B.V.) experienced in the respective modality. The PET images were analyzed by H.E.

The MR and PET readers were blinded to each other.

All MR images were analyzed with a workstation (AutoRad Diagnostic 4.2 Eastman Kodak).

The classification of the lymph nodes as non-malignant or malignant was based only on the pattern of nodal enhancement after USPIO administration following a modification of method described by Koh et al. [15].

The nodal size was not used in the classification of lymph nodes as nonmalignant or malignant.

The lymph nodes recognized on USPIO MR were categorized in three patterns:

1. Normal morphology with uniform or central signal drop (categorized as normal) (Figs. 1a, 2, 3).
2. Normal morphology without or with partial signal drop (categorized as total or partial invasion) (Figs. 1b, 5, 6).
3. Focal or global volume increase without or with partial signal drop (categorized as total invasion or partial invasion) (Figs. 1c, 4).

The performance of each sequence was assessed by comparing the number of pathological and normal lymph nodes recognized on a given sequence with the histology results on a patient basis.

For this evaluation the radiologists were blinded to the other sequences.

Surgery and histopathologic correlation

Surgery was performed in the range of 0 to 6 days. For the purpose of histopathologic correlation, a lymph node was regarded as positive for malignancy when tumor cells were present at light microscopy.

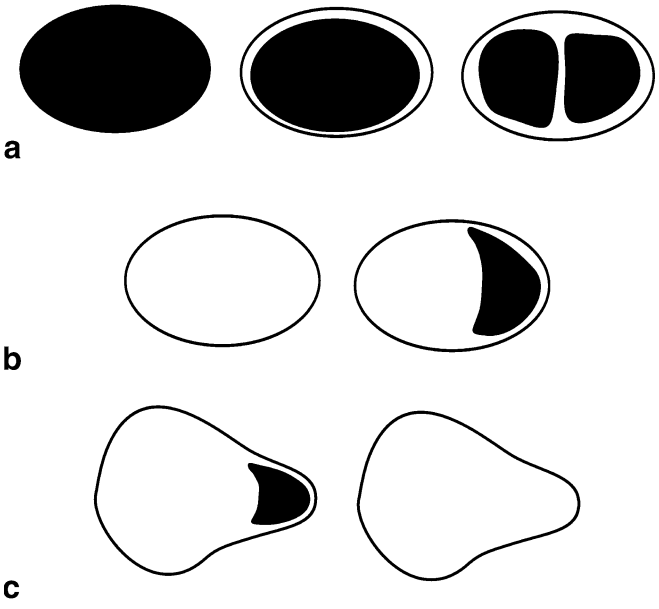

Fig. 1 a–c Patterns used for categorizations of lymph nodes as normal or invaded. **a** Normal morphology with uniform or central signal drop (categorized as normal). **b** Normal morphology without or with partial signal drop (categorized as total or partial invasion). **c** Focal or global volume increase without or with partial signal drop (categorized as total invasion or partial invasion)

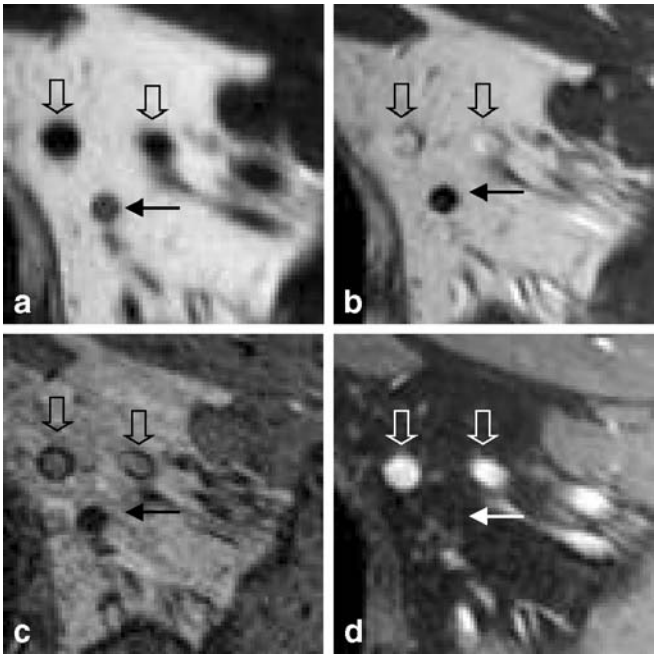

Fig. 2 a–d Ductal invasive breast carcinoma with normal axillary lymph nodes on histology, USPIO MR and FDG-PET. *Solid arrow* lymph node regarded as normal, *open arrows* blood vessels. **a** USPIO-enhanced T2-weighted 2D spin-echo image. There is no clear signal difference between the lymph node, blood vessels and muscle. **b** USPIO-enhanced T1-weighted 3D gradient echo. The signal intensity decrease with respect to the muscle is more obvious. The blood vessels are hyper intense (inflow enhancement). **c** USPIO-enhanced T2*-weighted 2D gradient echo. The signal intensity decrease is obvious. The blood vessels may be mistaken for invaded or fatty lymph nodes. **d** USPIO and gadolium-enhanced T1-weighted 3D gradient echo with spectral fat saturation. The normal lymph nodes are "switched-off" on this sequence. The blood vessels are hyperintense

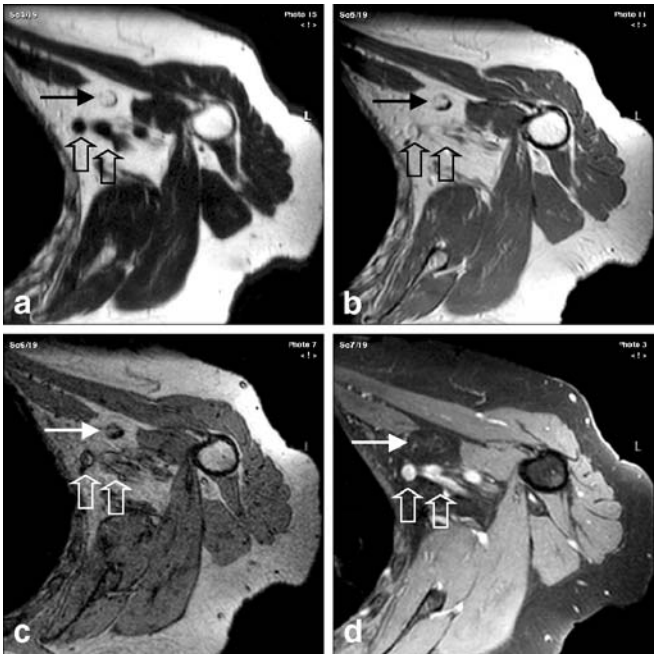

Fig. 3 a–d The same patient as in Fig. 2; lymph node regarded as normal with fatty sinus. *Solid arrow* normal lymph node, *open arrows* blood vessels. **a** USPIO-enhanced T2-weighted 2D spin-echo image. **b** USPIO-enhanced T1-weighted 3D gradient echo. The differentiation between fatty lymph node and blood vessels is problematic. **c** USPIO-enhanced T2*-weighted 2D gradient echo. The differentiation between fatty and centrally invaded lymph node is problematic. **d** USPIO and gadolium-enhanced T1-weighted 3D gradient echo with spectral fat saturation. The normal fatty lymph node is also "switched-off" on this sequence. The blood vessels are hyper intense

Because a node-to-node correlation between MR imaging and histological findings is difficult after axillary dissection, the statistical parameters were calculated on a patient basis (i.e., the result was considered as negative or positive for lymph node invasion independently of the number of invaded lymph nodes). Furthermore this correlation is impossible for PET imaging.

Statistical analysis

The Bayesian parameters of sensitivity, specificity, positive and negative predictive values, and diagnostic accuracy were calculated on a patient basis.

The number of invaded and normal lymph nodes provided by histopathologic evaluation was used to evaluate the performance of each sequence in detection of invaded and normal lymph nodes.

The closest match was assigned 4 points and the lowest, 1.

Results

The mean age of the study participants was 56 years and the age range was 41–74 years. The mean tumor size on histological analysis was 1.7 cm (range 1–3 cm).

On histological analysis, there were 5 patients with invaded axillary lymph nodes (in total 62 invaded and 38 normal lymph nodes)(diffuse invasion in all five, with concomitant micrometastes in two) and five without invasion (in total 62 normal lymph nodes).

On USPIO MR there was one false positive result and no false negative.

On FDG-PET there was one false negative result and no false positive.

The sensitivity, specificity, positive and negative predictive values calculated on a patient basis were, respectively, 100%, 80%, 80%, 100% for USPIO MR and 80%, 100%, 100%, 80% for FDG-PET. For these ten patients, the combination of USPIO MR with FDG-PET provided an overall accuracy of 100%.

For a total of 62 invaded lymph nodes reported on histological analysis, 42 were classified as invaded on gadolinium-enhanced T1-weighted 3D gradient echo with fat saturation, 35 on T2*-weighted 2D gradient echo, 31 on

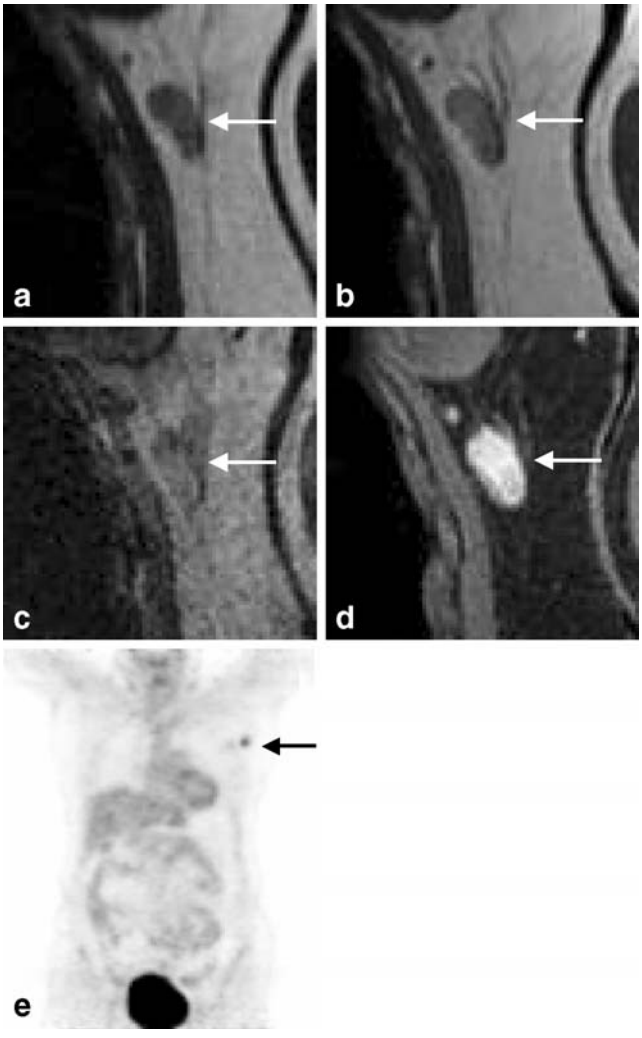

Fig. 4 a–e Ductal invasive breast carcinoma with invaded axillary lymph nodes on histology, USPIO MR and FDG-PET. *Solid arrow* invaded lymph node. **a** USPIO-enhanced T2-weighted 2D spin-echo image. The invaded lymph node is slightly more intense than the muscle. **b** USPIO-enhanced T1-weighted 3D gradient echo. The signal intensity increase with respect to the muscle is more obvious. **c** USPIO-enhanced T2*-weighted 2D gradient echo. The invaded lymph node is nearly isointense with the fat and therefore may be overlooked. **d** USPIO- and gadolium-enhanced T1-weighted 3D gradient echo with spectral fat saturation. The invaded lymph node shows important enhancement (switched-on). (**e**) FDG-PET shows pathological uptake of tracer (*black arrow*)

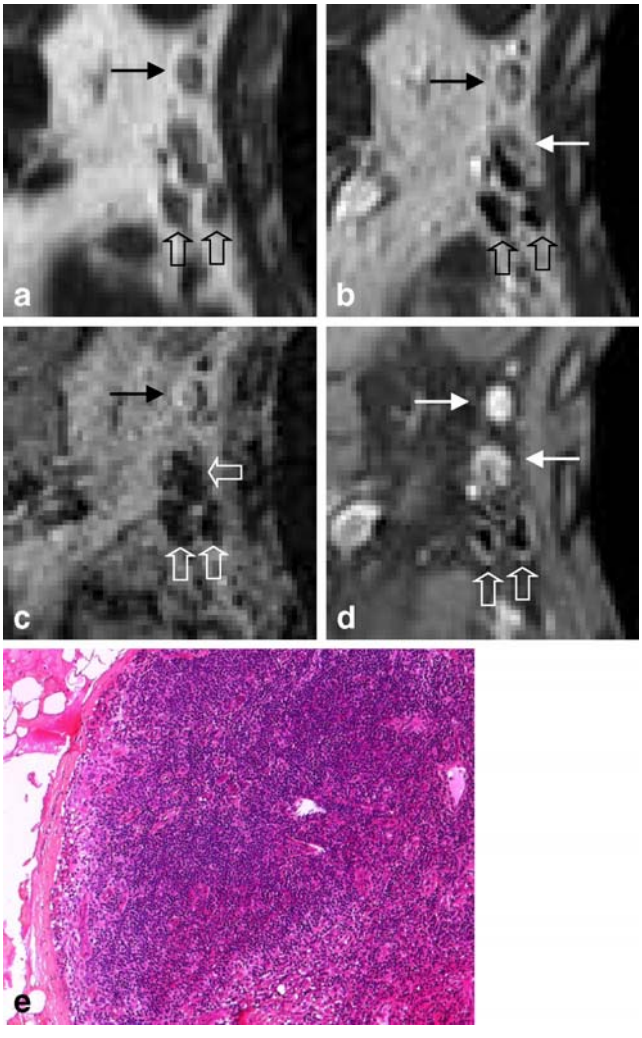

Fig. 5 a–e Lobular invasive breast carcinoma with normal axillary lymph nodes on histology and FDG-PET. Two lymph nodes were categorized as invaded on USPIO MR. *Solid arrow* false positive lymph node, *open arrows* true negative lymph nodes. **a** USPIO-enhanced T2-weighted 2D spin-echo image. The lymph nodes are more intense than the muscle. **b** USPIO-enhanced T1-weighted 3D gradient echo. There are two "bright" lymph nodes (*solid arrows*) and two with signal intensity drop. **c** USPIO-enhanced T2*-weighted 2D gradient-echo. There is one "bright" lymph node (*solid arrow*) and three with signal intensity drop. **d** USPIO- and gadolium-enhanced T1-weighted 3D gradient-echo with spectral fat saturation. There are two "bright" lymph nodes (*solid arrows*) and two with signal intensity drop. (**e**) Photomicrograph of histological specimen shows important inflammatory infiltration of the node by histiocytes (hematoxylin-eosin stain; original magnification, ×5.)

T1-weighted 3D gradient echo and 20 on T2-weighted 2D spin echo.

On FDG-PET, nine lesions were reported for a total of 59 invaded lymph nodes on histological analysis (four patients, one false negative result).

The most useful sequences in the detection of invaded lymph node were in the decreasing order:

– Gadolinium-enhanced T1-weighted 3D gradient echo with fat saturation
– T2*-weighted 2D gradient echo
– T1-weighted 3D gradient echo
– T2-weighted 2D spin echo

For a total of 100 normal lymph nodes reported on histological analysis, 79 were classified as normal on T2*-weighted 2D gradient echo, 59 on T1-weighted 3D gradient echo, 51 on gadolinium-enhanced T1-weighted

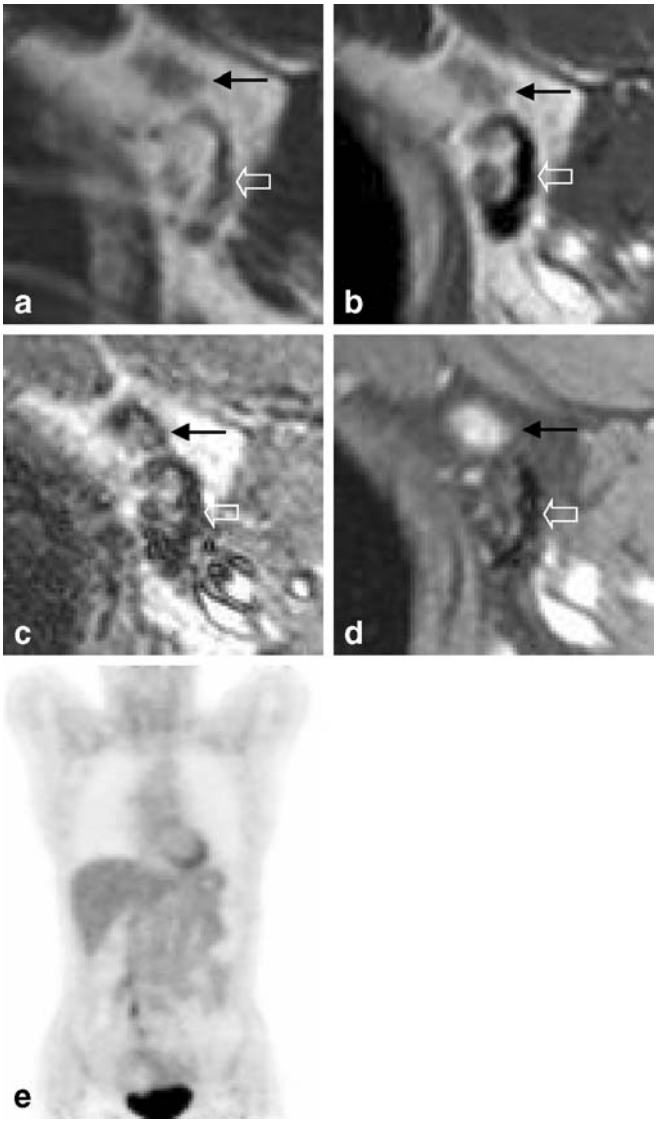

Fig. 6 **a–e** Lobular invasive breast carcinoma and ductal carcinoma in situ (DCIS) with invaded axillary lymph nodes on histology and on USPIO MR. False negative result of FDG-PET. *Solid arrow* lymph node categorized as invaded, *open arrow* lymph node categorized as normal. **a** USPIO-enhanced T2-weighted 2D spin-echo image. There is no clear signal intensity difference between the two lymph nodes. **b** USPIO-enhanced T1-weighted 3D gradient echo. The smaller, anterior lymph node is "bright," while the more posterior lymph node is much larger, with fatty sinus and shows signal intensity drop. **c** USPIO-enhanced T2*-weighted 2D gradient-echo. The difference between the two nodes is less clear due to the motion artefacts. **d** USPIO- and gadolium-enhanced T1-weighted 3D gradient echo with spectral fat saturation. The anterior lymph node is "bright" while the posterior one is "switched off". **e** FDG-PET shows no pathological uptake of tracer

3D gradient echo with fat saturation and 39 on T2-weighted 2D spin echo.

The most useful sequences in the detection of normal lymph node were in the decreasing order:

- T2*-weighted 2D gradient echo
- T1-weighted 3D gradient echo
- Gadolinium-enhanced T1-weighted 3D gradient echo with fat saturation
- T2-weighted 2D spin echo

Discussion

The accuracy of any imaging modality used to assess axillary nodes must closely match that of histopathologic findings.

The Gray scale and power Doppler US may provide the sensitivity, specificity, positive predictive value and negative predictive value in the range of 90% [16].

The reported accuracy of USPIO-enhanced MR (Sinerem, Guerbet, Roissy, France and Combidex, Advanced Magnetics, Boston, Mass.) in the detection of normal and invaded lymph node is superior to the results of morphologic evaluation, but remains insufficient with respect to the histopathologic findings.

Koh et al. [15] found a sensitivity of 66% (four of six), a specificity of 96% (65 of 68), a positive predictive value of 57% (four of seven), and a negative predictive value of 97% (65 of 67) in the evaluation of mesorectal lymph nodes. Mack et al. [17] reported similar results in the evaluation of head and neck lymph nodes, with the sensitivity of 86% (59 of 69), a specificity of 100% (960 of 960), a positive predictive value of 100% (59 of 59), and a negative predictive value of 99% (960 of 970). Michel et al. [13] found a sensitivity of 82% (nine of 11), a specificity of 100% (seven of seven), a positive predictive value of 100% (nine of nine), and a negative predictive value of 82% (nine of 11) in the preoperative breast cancer staging of 18 patients.

In our series of ten USPIO MRs, there was one false positive result that reduced the specificity and positive predictive value to 80%. This finding may be related to the reduced timing of the USPIO MR (in this particular study the time between the Sinerem injection and the USPIO MR was reduced to 20 h).

The optimal time for the postcontrast imaging with ferumoxtran-10 is 24–36 h, as established by early animal and human studies [18, 19]. This time lag before performing the postcontrast imaging is essential to allow sufficient extraction of ferumoxtran-10 by normal functioning macrophages within the nodes. If imaging is performed prematurely, the lack of sufficient nodal uptake within benign nodes may lead to erroneous characterization as malignant nodes (Fig. 5a–d).

The history of the recent breast surgery that induced an inflammatory infiltration of the lymph nodes (as confirmed

by the histology) may be another factor responsible for this false positive result (Fig. 5e).

Indeed, in the study of Koh et al. [15] the reactive lymph nodes were also responsible for three false positive results.

The reported accuracy of PET in the detection of normal and invaded lymph node is variable. Lovrics et al. [20] reported the sensitivity of 40% and the specificity of 97% in 98 patients. He concluded that PET scanning cannot replace histological staging in early stage breast cancer. The low rate of false-positive findings suggests that PET can identify women who can forego sentinel lymph node biopsy and require full axillary dissection.

Byrne et al. [21] reviewed the articles related to the assessment of the possible role of PET in the diagnosis and staging of breast cancer. In axillary staging, sensitivities of between 25 and 100% have been reported, but with a false negative rate of up to 20%. He concluded that PET is not a single diagnostic and staging tool that can replace current surgical, histological and radiological staging.

In our series, there was one false negative result for FDG PET with overall sensitivity and negative predictive value of 80%.

The acquisition strategies may include or not a pre-contrast MR study intended to evaluate the signal decrease after USPIO injection. Several studies have demonstrated significant signal decrease after USPIO injection in normal lymph nodes on T2*-weighted gradient-echo sequences and to a less extent on T1-weighted gradient-echo sequences [11, 12, 17, 22–25].

However, this strategy implies the multiplication of MR examinations. Furthermore, the very good accuracy in the USPIO detection of normal and invaded lymph node was also achieved in the studies without pre-USPIO MR [13].

Therefore, in our study the MR imaging was not performed before the administration of USPIO.

If the gadolinium-enhanced MR of the breast may be combined with USPIO-enhanced MR of the axillary lymph nodes, one step preoperative breast cancer staging with MR imaging becomes possible. Michel et al. [13] demonstrated that USPIO administration shows no clinically relevant interference with dynamic gadolinium-enhanced MR imaging of the breast. Thus, both USPIO-enhanced MR imaging of the axilla and gadolinium-enhanced MR imaging of the primary tumor can be performed within the same imaging session.

Moreover, Luciani et al. [5] reported significantly higher enhancement in the invaded lymph nodes than in those with negative pathologic findings.

Therefore, we tried to evaluate if the additional injection of gadolinium may be useful in the differentiation of normal and invaded lymph node on USPIO-enhanced MR imaging. In our experience, all lymph nodes classified as malignant on T2*-weighted 2D gradient echo and T1-weighted 3D gradient echo showed enhancement on post-gadolinium T1 weighted 3D gradient echo with fat saturation. The lymph nodes classified as normal were dark (Fig. 2a–d) or showed only a fine, peripheral rim of enhancement (Figs. 3a–d, 5d *white open arrows*), while the invaded lymph nodes showed important enhancement (Fig. 4a–d).

We speculate that the strong dephasing of protons induced by USPIO particles is responsible for this behaviour on T1-weighted gradient-echo sequence.

In our experience, this behaviour has never been tested nor reported in the literature.

As both invaded lymph nodes and vessels are similarly high in signal intensity on T2*-weighted images, they may be mistaken for one another. Hence, both T2- and/or T1- and T2*-weighted imaging are performed for the assessment of lymph nodes [15].

In our experience, the gadolinium-enhanced T1-weighted 3D gradient echo with fat saturation was superior to T2*-weighted gradient echo in the detection of completely invaded malignant lymph node. The completely invaded lymph node may be overlooked on T2* gradient echo due to the lack of contrast with the surrounding fat, while on gadolinium-enhanced T1-weighted 3D gradient echo with fat saturation, the pathological lymph node "switch on".

A node-to-node comparison between USPIO-enhanced MR imaging and histopathologic findings was not possible because of the block resection and the few reference structures in the axilla. This correlation is particularly difficult for small nodes. MR imaging-guided axillary node biopsy should be considered in the future [26]. Furthermore, this correlation is impossible for FDG PET studies. Because in our study the MR imaging was not performed before the administration of USPIO, it is also not proven whether the USPIO enhancement is necessary to ensure the high sensitivity achieved by gadolinium-enhanced T1-weighted fat saturation sequence.

In addition, the issue of the micrometastases represents a significant problem with imaging, particularly with PET scan. It is probably that the problem of the false negative results in case of the micrometastases will not be solved with MR imaging and PET.

Conclusions

1. The combination of USPIO-enhanced MR and FDG-PET has the potential to accurately assess axillary lymph node status and modify the preoperative assessment of axillary lymph nodes in breast cancer, including the indications for sentinel node lymphadenectomy. The combination of USPIO MR with FDG-PET provided 100% sensitivity, specificity, PPV and NPV. If these results are confirmed, the combination of USPIO MR with FDG-PET has the potential to identify candidate patients for axillary dissection versus sentinel node lymphadenectomy. However,

owing to the small number of patients, these data have to be considered as "under investigation" until more data are available.

2. In our study, USPIO-enhanced T1 gradient echo after gadolinium injection and fat saturation emerged as a very useful sequence in the staging of invaded lymph nodes and should be included in the USPIO-enhanced preoperative assessment of axillary lymph nodes.

This finding suggests that the gadolinium-enhanced MR of the breast may be combined with USPIO-enhanced MR of the axillary lymph nodes in one-step preoperative breast cancer staging.

References

1. Morrow M (1996) Role of axillary dissection in breast cancer management. Ann Surg Oncol 3:233–234
2. Mancuso AA, Maceri D, Rice D, Hanafee W (1981) CT of cervical lymph node cancer. AJR Am J Roentgenol 136:381–385
3. Som PM (1987) Lymph nodes of the neck. Radiology 165:593–600
4. Steinkamp HJ, Cornehl M, Hosten N, Pegios W, Vogl T, Felix R (1995) Cervical lymphadenopathy: ratio of long- to short-axis diameter as a predictor of malignancy. Br J Radiol 68:266–270
5. Luciani A, Dao TH, Lapeyre M, Schwarzinger M, Debaecque C, Lantieri L, Revelon G, Bouanane M, Kobeiter H, Rahmouni A (2004) Simultaneous bilateral breast and high-resolution axillary MRI of patients with breast cancer: preliminary results. AJR Am J Roentgenol 182:1059–1067
6. Brown G, Richards CJ, Bourne MW, Newcombe RG, Radcliffe AG, Dallimore NS, Williams GT (2003) Morphologic predictors of lymph node status in rectal cancer with use of high-spatial-resolution MR imaging with histopathologic comparison. Radiology 227:371–377
7. Anzai Y, Blackwell KE, Hirschowitz SL et al (1994) Initial clinical experience with dextran-coated superparamagnetic iron oxide for detection of lymph node metastases in patients with head and neck cancer. Radiology 192:709–715
8. Bellin MF, Roy C, Kinkel K et al (1998) Lymph node metastases: safety and effectiveness of MR imaging with ultrasmall superparamagnetic iron oxide particles-initial clinical experience. Radiology 207:799–808
9. Bellin MF, Beigelman C, Precetti-Morel S (2000) Iron oxide-enhanced MR lymphography: initial experience. Eur J Radiol 34:257–264
10. Anzai Y, McLachlan S, Morris M, Saxton R, Lufkin RB (1994) Dextran-coated superparamagnetic iron oxide, an MR contrast agent for assessing lymph nodes in the head and neck. AJNR Am J Neuroradiol 15:87–94
11. Anzai Y, Prince MR (1997) Iron oxide-enhanced MR lymphography: the evaluation of cervical lymph node metastases in head and neck cancer. J Magn Reson Imaging 7:75–81
12. Harisinghani MG, Saini S, Slater GJ, Schnall MD, Rifkin MD (1997) MR imaging of pelvic lymph nodes in primary pelvic carcinoma with ultrasmall superparamagnetic iron oxide (Combidex): preliminary observations. J Magn Reson Imaging 7:161–163
13. Michel SC, Keller TM, Frohlich JM, Fink D, Caduff R, Seifert B, Marincek B, Kubik-Huch RA (2002) Preoperative breast cancer staging: MR imaging of the axilla with ultrasmall superparamagnetic iron oxide enhancement. Radiology 225:527–536
14. Stets C, Brandt S, Wallis F, Buchmann J, Gilbert FJ, Heywang-Kobrunner SH (2002) Axillary lymph node metastases: a statistical analysis of various parameters in MRI with USPIO. J Magn Reson Imaging 16:60–68
15. Koh DM, Brown G, Temple L, Raja A, Toomey P, Bett N, Norman AR, Husband JE (2004) Rectal cancer: mesorectal lymph nodes at MR imaging with USPIO versus histopathologic findings-initial observations. Radiology 231:91–99
16. Esen G, Gurses B, Yilmaz MH et al (2005) Gray scale and power Doppler US in the preoperative evaluation of axillary metastases in breast cancer patients with no palpable lymph nodes. Eur Radiol 15:1215–1223
17. Mack MG, Balzer JO, Straub R, Eichler K, Vogl TJ (2002) Superparamagnetic iron oxide-enhanced MR imaging of head and neck lymph nodes. Radiology 222:239–244
18. Weissleder R, Elizondo G, Wittenberg J, Lee AS, Josephson L, Brady TJ (1990) Ultrasmall superparamagnetic iron oxide: an intravenous contrast agent for assessing lymph nodes with MR imaging. Radiology 175:494–498
19. Bordat C, Sich M, Rety F et al (2000) Distribution of iron oxide nanoparticles in rat lymph nodes studied using electron energy loss spectroscopy (EELS) and electron spectroscopic imaging (ESI). J Magn Reson Imaging 12:505–509
20. Lovrics PJ, Chen V, Coates G, Cornacchi SD, Goldsmith CH, Law C, Levine MN, Sanders K, Tandan VR (2004) A prospective evaluation of positron emission tomography scanning, sentinel lymph node biopsy, and standard axillary dissection for axillary staging in patients with early stage breast cancer. Ann Surg Oncol 11:846–853
21. Byrne AM, Hill AD, Skehan SJ, McDermott EW, O'Higgins NJ (2004) Positron emission tomography in the staging and management of breast cancer. Br J Surg 91:1398–1409. Review
22. Hoffman HT, Quets J, Toshiaki T et al (2000) Functional magnetic resonance imaging using iron oxide particles in characterizing head and neck adenopathy. Laryngoscope 110:1425–1430
23. Sigal R, Vogl T, Casselman J et al (2002) Lymph node metastases from head and neck squamous cell carcinoma: MR imaging with ultrasmall superparamagnetic iron oxide particles (Sinerem MR)-results of a phase-III multicenter clinical trial. Eur Radiol 12:1104–1113
24. Nguyen BC, Stanford W, Thompson BH et al (1999) Multicenter clinical trial of ultrasmall superparamagnetic iron oxide in the evaluation of mediastinal lymph nodes in patients with primary lung carcinoma. J Magn Reson Imaging 10:468–473
25. Pannu HK, Wang KP, Borman TL, Bluemke DA (2000) MR imaging of mediastinal lymph nodes: evaluation using a superparamagnetic contrast agent. J Magn Reson Imaging 12:899–904
26. Yamagami T, Yuen S, Sawai K, Nishimura T (2004) MR imaging-guided axillary node biopsy for breast cancer: initial findings. Eur Radiol 14:151–156